Thioredoxin-interacting protein deficiency disrupts the fasting-feeding metabolic transition

Sonal S. Sheth,* Lawrence W. Castellani,* Soumya Chari,* Cory Wagg,† Christopher K. Thipphavong,* Jackie S. Bodnar,* Peter Tontonoz,§ Alan D. Attie, Gary D. Lopaschuk,† and Aldons J. Lusis[1],***

Departments of Human Genetics, Medicine, Molecular Biology Institute, and Microbiology, Immunology, & Molecular Genetics,* University of California, Los Angeles, David Geffen School of Medicine at UCLA, Los Angeles, CA 90095; Faculty of Medicine and Dentistry,† University of Alberta, Edmonton, Alberta, Canada T6G 2S2; Molecular Biology Institute,§ Howard Hughes Medical Institute, Department of Pathology and Laboratory Medicine, University of California, Los Angeles, CA 90095; and Department of Biochemistry,** University of Wisconsin-Madison, Madison, WI 53706

Abstract **Through a positional cloning approach, the thioredoxin-interacting protein gene (*Txnip*) was recently identified as causal for a form of combined hyperlipidemia in mice (Bodnar, J. S., A. Chatterjee, L. W. Castellani, D. A. Ross, J. Ohmen, J. Cavalcoli, C. Wu, K. M. Dains, J. Catanese, M. Chu, S. S. Sheth, K. Charugundla, P. Demant, D. B. West, P. de Jong, and A. J. Lusis. 2002. Positional cloning of the combined hyperlipidemia gene Hyplip1. *Nat. Genet.* 30: 110–116). We now show that Txnip-deficient mice in the fed state exhibit a metabolic profile similar to fasted mice, including increased levels of plasma ketone bodies and free fatty acids, decreased glucose, and increased hepatic expression of peroxisome proliferator-activated receptor-γ coactivator-1α, phosphoenolpyruvate carboxykinase, glucose-6-phosphatase, and acyl-CoA oxidase. Dramatic differences in the expression of key metabolic enzymes were also observed in other tissues, and the fat-to-muscle ratio of Txnip-deficient mice was increased by ~40%. We demonstrate an effect of Txnip on the redox status, as the Txnip-deficient mice in the fed state had a significant increase in the ratio of NADH to NAD^+. Surprisingly, we observed that Txnip-deficient mice and wild-type mice had similar levels of thioredoxin activity, suggesting that the effects of Txnip deficiency may be mediated in part by other interactions. These results indicate a role for Txnip in the metabolic response to feeding and the maintenance of the redox status.**—Sheth, S. S., L. W. Castellani, S. Chari, C. Wagg, C. K. Thipphavong, J. S. Bodnar, P. Tontonoz, A. D. Attie, G. D. Lopaschuk, and A. J. Lusis. **Thioredoxin-interacting protein deficiency disrupts the fasting-feeding metabolic transition.** ***J. Lipid Res.*** **2005.** 46: **123–134.**

Supplementary key words redox status • nutritional status • hypoglycemia • hypertriglyceridemia • fatty acid oxidation • mice

We previously identified a naturally occurring mouse model for familial combined hyperlipidemia, a disorder characterized by increased plasma cholesterol and triglycerides (1). Subsequently, positional cloning showed that the hyperlipidemia resulted from a spontaneous nonsense mutation in the gene for thioredoxin-interacting protein (*Txnip*), also known as vitamin D_3 upregulated protein 1 (2). Txnip was originally identified in a yeast two-hybrid screen for proteins that bind to thioredoxin (Txn), a thiol oxidoreductase that undergoes NADPH-dependent reduction and has multiple roles in intracellular signaling and resistance to oxidative stress (3–6). The nonsense mutation in the hyperlipidemic mouse resulted in dramatically reduced mRNA levels and a truncated Txnip peptide lacking the region of the C terminus required for Txn binding (2). We showed that Txnip-deficient mice exhibited increased production of triglyceride-rich lipoproteins and ketone bodies. Liver slices isolated from Txnip-deficient mice also exhibited reduced hepatic CO_2 production, suggesting an impairment of the tricarboxylic acid (TCA) cycle. We proposed that the Txnip deficiency reduced flux through the TCA cycle, sparing fatty acids for incorporation into triglycerides and ketone bodies (2). Because the only known function of Txnip was binding to and inhibiting Txn, we speculated that the Txnip-deficient mice would exhibit increased Txn activity and an imbalance of the cellular redox state, perhaps resulting in increased NADH levels, which could lead to the downregulation of the TCA cycle (2).

Abbreviations: AOX, acyl-CoA oxidase; ECL, enhanced chemiluminescence; Glut2, glucose transporter 2; G6Pase, glucose-6-phosphatase; KH, Krebs-Henseleit; MCAD, medium-chain acyl-CoA dehydrogenase; p-CREB, phosphorylated cAMP response element binding protein; PEPCK, phosphoenolpyruvate carboxykinase; PGC-1α, peroxisome proliferator-activated receptor-γ coactivator-1α; SCD1, stearoyl-CoA desaturase 1; SREBP-1c, sterol-response element binding protein-1c; TCA, tricarboxylic acid; TNFα, tumor necrosis factor-α; Txn, thioredoxin; Txnip, thioredoxin-interacting protein.

[1] To whom correspondence should be addressed.
e-mail jlusis@mednet.ucla.edu

Manuscript received 9 September 2004 and in revised form 21 October 2004.

Published, JLR Papers in Press, November 1, 2004.
DOI 10.1194/jlr.M400341-JLR200

Subsequently, Donnelly et al. (7) used stable isotope methods to demonstrate that Txnip-deficient mice exhibit increased lipogenesis and increased hepatic triglyceride and cholesterol ester stores. Recently, Hui et al. (8) reported that fasted Txnip-deficient mice had depressed glucose levels and that the ablation of pancreatic β cells by treatment with streptozotocin reduced the hypertriglyceridemia phenotype, suggesting that increased insulin secretion may be a primary contributing factor to the metabolic alterations. They also presented evidence that the hypertriglyceridemia resulted in part from increased expression of the lipogenic transcription factor sterol-response element binding protein-1c (SREBP-1c) (8). Schulze et al. (9) presented evidence that the oxidative stress contributing to the complications of diabetes may be mediated in part by the induction of Txnip by increased glucose.

We now report metabolic studies of Txnip-deficient mice in the fed and fasted states. We observed profound alterations in both lipid and glucose metabolism in multiple tissues despite the absence of significant differences in insulin levels, suggesting direct metabolic effects of Txnip in liver, heart, and adipose. In several respects, the metabolic profile of fed Txnip-deficient mice resembles that of mice subjected to prolonged fasting. One regulatory factor that appears to be involved is the transcriptional coactivator, peroxisome proliferator-activated receptor-γ coactivator-1α (PGC-1α), whose expression is significantly increased in the Txnip-deficient mice in the fed state. We have also examined mechanisms mediating the effects of Txnip deficiency. We observed a significant increase of NADH in fed Txnip-deficient mice, consistent with an effect on the redox status, but surprisingly, the activity of Txn was not significantly increased. Our results indicate that Txnip is required for appropriate metabolic responses to feeding.

EXPERIMENTAL PROCEDURES

Animal husbandry and diets

The development of the recombinant congenic mutant mouse strain HcB-19/*Dem*, recombinant inbred strains, and congenic strains were described previously (1, 2, 10). To study the effects of the *Txnip* mutation on various backgrounds, all mice were housed under conditions meeting the guidelines of the Association for Assessment and Accreditation of Laboratory Animal Care and were housed in groups of five or fewer animals per cage and maintained on a 12 h light-dark cycle at an ambient temperature of 23°C. They were allowed ad libitum access to water and rodent chow containing 6% fat (Diet No. 8604; Harlan Teklad, Madison, WI). For the studies conducted in the fasted state, samples were obtained at ~12:00 noon after an overnight fast. All animal care and experimental protocols were approved by the University of California, Los Angeles Animal Research Committee.

Body composition

Fat-to-muscle mass ratio was determined using NMR spectroscopy. The NMR instrument (Bruker Biospin, Billerica, MA) was calibrated according to the manufacturer's instructions. To measure body composition, Txnip-deficient and wild-type mice were individually contained in a cylinder and placed in the instrument. The amount of total body mass was determined as the sum of fat mass, lean mass, and water.

Plasma lipid, ketone body, lactate, glucose, insulin, and leptin determinations

Mice were either fed ad libitum or fasted for 18 h before retroorbital bleeding, and were bled under isofluorane anesthesia using EDTA as the anticoagulant. Plasma lipids were determined as described previously (11). To minimize the hydrolysis of triglycerides, the blood samples were immediately placed on ice, centrifuged to separate the plasma, and frozen. To validate the FFA assay, we also measured free glycerol from the triglycerides between the two strains. There was no significant difference in glycerol levels, indicating that the increased FFA in Txnip-deficient mice is not attributable to in vitro hydrolysis. Levels of the ketone body β-hydroxybutyrate were determined in duplicate using a kit (#310-A; Sigma). Blood collection tubes were prechilled on ice, and the samples were centrifuged within 5 min to remove erythrocytes to obtain accurate plasma lactate concentrations, which were measured in duplicate using a lactate kit (#735-10; Sigma). Plasma glucose concentrations were measured in triplicate using a glucose kit (#315-100; Sigma). For glucose measurements, blood collection tubes were prechilled on ice and the samples centrifuged within 5 min to minimize glucose metabolism by erythrocytes. Plasma insulin levels were determined in duplicate by sensitive rat insulin RIA (SRI-13K; LINCO Diagnostics) and ELISA (#008-10-1150-01; ALPCO Diagnostics). Plasma leptin levels were measured in duplicate using a mouse ELISA kit (#MOB00; R&D Systems).

Hepatic glycogen levels

Liver tissue samples were homogenized in double-distilled H_2O. Aliquots of the homogenate were transferred to an acetate buffer solution containing 50 μg of α-glucosidase (#A7420; Sigma) and 2.7 μl of α-amylase (#A4268; Sigma) per milliliter of buffer solution. Aliquots of homogenates were also transferred to acetate buffer solution containing no enzymes to serve as a sample blank. A standard curve was generated with a serial dilution of glucose. After addition to the buffer solution, the tubes were incubated at 37°C for 10 min and centrifuged in a microcentrifuge for 5 min at 3,000 rpm, and 170 μl of the supernatant, in triplicate, was transferred to a 96-well plate and read at 490 nm in a Molecular Devices Spectramax plus microplate reader.

Glucose and fatty acid oxidation in the heart

The University of Alberta Health Sciences Laboratory Animal Services and Welfare Committee approved all animal procedures and conformed to the guidelines of the Canadian Council on Animal Care. Experiments were done as previously described (12). Txnip-deficient and wild-type mice (25–30 g) were heparinized (100 units ip) 10 min before anesthetizing with 50 μl ip of sodium pentobarbital. The heart was quickly removed and submerged in ice-cold Krebs-Henseleit (KH) solution (118 mM NaCl, 4.7 mM KCl, 1.2 mM KH_2PO_4, 1.2 mM $MgSO_47H_2O$, 2.5 mM $CaCl_22H_2O$, and double-distilled H_2O). The mouse heart was cannulated in two stages. *1*) The lungs were removed and the aorta was cannulated on a modified 20 gauge catheter syringe, after which a retrograde perfusion was initiated with 37°C KH solution at 60 mmHg hydrostatic pressure. The aorta was sutured to the cannula, and the heart was observed for a pulse before performing the next stage. *2*) The catheter and heart were removed from the injection port and moved to the main cannula. Here, the remaining excess tissue was removed and the left atrium was cannulated and sutured. After this, the Langendorff line was clamped and the hearts were perfused at 11 mmHg left atrial preload and 50 mmHg aortic afterload. The working KH

solution contained 5 mM glucose, 25 mM $NaHCO_3$, 3% fatty acid-free BSA (Equitech-Bio, Inc.), 1.2 mM palmitate bound to the BSA, 100 μU/ml human biosynthetic insulin (Novo Nordisk, Inc.), [U-^{14}C]glucose, and [9,10-^{3}H(N)]palmitate. Hyamine hydroxide (1 M; Curtiss Laboratories, Inc.) was used to capture the $^{14}CO_2$ produced by the heart, as described. The hearts were perfused for 30 min aerobically. Buffer (5 ml) and hyamine (2 × 300 μl) samples were removed every 10 min. At the end of the protocol, the ventricle was isolated, cut down, and instantly frozen in liquid N_2. The remaining atria was taken down, dried, and used for total dry weight of the heart. Glucose oxidation was determined by the quantitative collection of $^{14}CO_2$ produced from D-[U-^{14}C]glucose (Amersham Biosciences). At every sample time, 5 ml of buffer was taken; 2 ml was used for the collection of $^{14}CO_2$, and the remaining 3 ml was placed under paraffin oil and used for the $^{3}H_2O$ extraction assay. Palmitate oxidation was measured quantitatively from [9,10-^{3}H]palmitate acid (Perkin-Elmer) from the collection of $^{3}H_2O$. 1.5 ml capless microfuge tubes (containing 200 μl of buffer sample) were placed in 7 ml capped scintillation vials containing 500 μl of H_2O and were incubated at 50°C for 24 h and then removed and cooled at 4°C overnight. This was done in duplicate. A standard of $^{3}H_2O$ (Sigma) was also prepared to find the percentage of $^{3}H_2O$ transferred in the heating and cooling process. The capless microfuge tubes were disposed of, and the scintillation vials were filled with 5 ml of Ecolite (ICN) scintillant and measured for activity.

Fatty acid oxidation in the soleus muscle

After an 18 h fast, C3H/DiSnA (wild-type) and Txnip-deficient mice were anesthetized with pentobarbital (50 mg/kg body weight), and the soleus muscle was isolated with a dissecting microscope. The muscles were weighed and immediately incubated for 40 min in KH buffer under 95% O_2/5% CO_2 that contained 5.5 mM glucose, 3% BSA, 1 mM palmitate, and [U-^{14}C]palmitic acid (2.5 μCi/ml). Rates of fatty acid oxidation were assessed by determining the radioactivity in $^{14}CO_2$ trapped in hyamine hydrochloride as described previously (13).

RNA analysis

Mice were either fed ad libitum or fasted for 18 h and were sacrificed by cervical dislocation. Total RNA was isolated from liver, gonadal fat pads, and skeletal muscle with TriZol reagent according to the manufacturer's instructions (Invitrogen). For RT-PCR analysis, first-strand cDNAs were synthesized with the use of 1 μg of total RNA isolated from the liver, gonadal fat pads, and skeletal muscle and the use of Taqman RT reagents (ABI). Taqman real-time quantitative PCR experiments were done using the Applied Biosystems 7700 sequence detector as previously described (14). Results are presented as averages of duplicate determinations normalized to 36B4 expression.

Western blot analyses

Mice were either fed ad libitum or fasted for 18 h and were sacrificed by cervical dislocation. Liver tissue was immediately removed and placed in liquid nitrogen. Frozen tissue was weighed and added to a lysis buffer (20 mM HEPES, 100 mM KCl, 300 mM NaCl, 10 mM EDTA, 0.1% Nonidet P-40, and a cocktail of protease inhibitors; Roche). For Western blot analysis, appropriate protein samples were reduced in DTT, boiled, electrophoresed on 10% SDS-PAGE gels, and electroblotted onto enhanced chemiluminescence (ECL) nitrocellulose membranes using a transfer apparatus from Invitrogen according to the manufacturer's instructions. Membranes were blocked with phosphate-buffered saline with 0.1% Tween 20/5% nonfat dry milk overnight, washed, and incubated with primary and secondary antibodies for 2 and 1 h, respectively. The primary antibodies for Txn (Santa Cruz Biotechnologies) and phosphorylated cAMP response element binding protein (p-CREB; Upstate) were commercially available antibodies. The secondary antibody used was horseradish peroxidase–conjugated anti-rabbit IgG for Txn and p-CREB (Amersham). Primary and secondary antibodies for Txn were used at 1:500 and 1:1,000 dilutions, respectively. For p-CREB, primary and secondary antibodies were used at 1:350 and 1:1,000 dilutions, respectively. The membranes were washed extensively with phosphate-buffered saline/0.1% Tween 20 after primary and secondary antibody incubation and detected using the ECL Western blotting kit (Amersham) according to the manufacturer's suggested protocol. Protein levels for Txn and p-CREB were normalized against β-actin and α-tubulin protein levels, respectively, to ensure equal loading. To generate an antibody against Txnip, several approaches yielded poor results. First, synthetic peptides against three different immunogenic regions of the protein were created; however, all were nonspecific. We then attempted to use a bacterial expression vector system to generate Txnip protein, but the protein appeared to be toxic to various strains of bacteria. We also were able, through the generous contributions of the Lee and Yodoi laboratories (9, 15), to obtain polyclonal antibodies against mouse and human Txnip. Unfortunately, in our hands, these also yielded nonspecific results.

Nucleotide determinations

Pyridine dinucleotide levels were determined as described elsewhere with slight modifications (16). Because of the lack of availability of C3H/DiSnA mice, C3H/HeJ mice were used as wild-type mice for these experiments. To ensure that the lipid profiles were similar, we measured the triglycerides in the C3H/HeJ mice used in the experiment. The average fasted triglyceride value in C3H/HeJ mice was 72.2 mg/dl, and the average triglyceride value in C3H/DiSnA mice was 68.8 mg/dl. Mice were either fed ad libitum or fasted for 18 h and were sacrificed by cervical dislocation. Liver tissue was immediately removed and freeze-clamped in liquid nitrogen. Seventy-five milligrams of frozen tissue was homogenized in 750 μl of extraction buffer (0.2 M potassium cyanide, 0.06 M potassium hydroxide, 1 mM bathophenanthrolinedisulfonic acid). Homogenate was extracted with chloroform and centrifuged for 6 min at 13,000 rpm. The supernatant was once again extracted with chloroform and centrifuged. The aqueous sample was filtered through a 0.45 μm positively charged nylon-55 filter. The sample was then diluted with 4 parts mobile phase (0.2 M ammonium sulfate, 4 mM tetrabutylammonium hydrogen sulfate, pH 6) and immediately applied to the HPLC machine. HPLC analysis used a Supelcosil LC-18-T column (Supelco) with a guard column. The HPLC program was as follows: after 1 min at 96% mobile phase and 4% methanol, the methanol increases at 0.8%/min for 25 min. The column was then flushed with water for 12 min, pure methanol for 18 min, and then water for another 12 min before returning to starting conditions. The flow rate was 1 ml/min, and the fluorescence was detected at an excitation wavelength of 330 nm and an emission wavelength of 460 nm.

Insulin-reducing assay for Txn activity

The insulin disulfide reduction assay was performed essentially as described elsewhere with slight modifications (17). Liver protein was isolated as described above. Twenty micrograms of protein was preincubated at 37°C for 20 min with 2 μl of DTT activation buffer (50 mM HEPES, pH 7.6, 1 mM EDTA, 1 mg/ml BSA, and 2 mM DTT) for a total volume of 10 μl. Forty microliters of reaction mixture, containing 200 μl of 1 M HEPES (pH 7.6), 40 μl of 0.2 M EDTA, 40 μl of NADPH (40 mg/ml), and 500 μl of insulin (10 mg/ml) were added. The reaction began with the addition of 10 μl of rat Txn reductase (100 A_{412} U/ml; Sigma), and

the incubation continued for 20 min at 37°C. The reaction was terminated with 0.5 ml of 6 M guanidine-HCl and 1 mM 3-carboxy-4-nitrophenyl disulfide, and the absorbance at 412 nm was measured. To control for other oxidoreductases, samples were treated with and without Txn reductase. Rat Txn (Sigma) was used to generate a standard curve ranging from 100 to 1,200 ng/ml.

Statistical analyses

Data are presented as means ± SEM, with n indicating the number of mice. The statistical significance of differences in plasma lipid levels, glucose and fatty acid oxidation, gene expression levels, protein and activity levels, and ratios between reduced and oxidized pyridine nucleotides between the two groups was determined with ANOVA. Differences were considered statistically significant at $P < 0.05$.

RESULTS

General characteristics of Txnip-deficient mice

We have now examined the Txnip-deficient mice on a variety of genetic backgrounds, including C3H/DiSnA, C57BL/10ScSnA, C57BL/6J, BALB/c, and CAST/Ei, and all exhibited similarly increased plasma triglyceride and ketone body levels. The experiments reported here were performed on mice with a C3H/DiSnA genetic background between 3 and 5 months of age. Txnip-deficient mice were similar in weight and activity to wild-type or heterozygous littermates, with no differences in food consumption (data not shown). The litter sizes of the Txnip-deficient mice were reduced, and in crosses involving heterozygous mice, lower than expected frequencies of Txnip-deficient mice were born (data not shown). We have also noted that some older Txnip-deficient mice, ~9 months of age or older, develop liver adenomas and carcinomas (S. S. Sheth, A. Ghazalpour, J. S. Bodnar, and A. J. Lusis, unpublished data).

Although Txnip-deficient mice are similar in weight to wild-type littermates, the proportion of fat to muscle mass is significantly different between the two groups. Using NMR analysis, the fat-to-muscle mass ratio was 1.4 times higher in Txnip-deficient mice than in wild-type mice (**Fig. 1A**). This was primarily attributable to a significant decrease in the muscle mass, which was confirmed by directly measuring the soleus muscle mass in Txnip-deficient mice (Fig. 1B).

Txnip-deficient mice exhibit an abnormal metabolic profile in the fed and fasted states

To define the metabolic profile of the Txnip-deficient mice, we measured various lipid and glucose metabolic parameters in the fed and fasted states. The Txnip-deficient mice exhibited increased levels of plasma ketone bodies, with an ~2-fold increase compared with wild-type mice in the fed state and a 6-fold increase in the fasted state (Fig. 1C). Plasma FFA levels, which if altered should be increased in the fasted state as a result of increased adipose tissue triglyceride lipolysis, were significantly increased in both the fed and fasted states in Txnip-deficient mice (Fig. 1D). Likewise, plasma glucose levels were reduced in both the fed and fasted states, the decrease being particularly prominent (53%) in the fasted state (Fig. 1E). Glycogen, which is metabolized in the fasted state, was also reduced in livers of the Txnip-deficient mice in the fasted state (Fig. 1F). Thus, several metabolic alterations associated with fasting, including increased ketone bodies, increased FFA, and decreased glucose levels, were all observed in Txnip-deficient mice in the fed state (Fig. 1).

Under normal physiologic conditions, there is a decrease in plasma triglyceride levels in the fasted state. However, the Txnip-deficient mice exhibited the opposite response, an increase in plasma triglycerides (Fig. 1G). We previously also showed that Txnip-deficient mice exhibit decreased flux through the TCA cycle in liver as judged by the production of CO_2 (2), which would spare fatty acids for incorporation into triglycerides. As discussed below, fatty acid synthase expression was also increased in Txnip-deficient mice. Plasma LDL and VLDL cholesterol levels were also higher in fasted Txnip-deficient mice (Fig. 1H).

Because there are clearly important metabolic interactions between liver, muscle, and adipose, it is likely that the decreased muscle mass contributes to the metabolic perturbations observed in livers of Txnip-deficient mice. Notably, the decreased muscle mass would influence glucose and triglyceride utilization. Interestingly, despite the decreased muscle mass, plasma lactate levels were increased. Plasma lactate levels were significantly higher, by ~55%, in the fed state of the Txnip-deficient mice (Fig. 1I). The increased plasma lactate, which represents the muscle equivalent of ketone bodies, may be explained in part by a decrease in pyruvate oxidation caused by increased fatty acids, resulting in pyruvate being redirected to lactate.

Plasma leptin levels were measured in the fed and fasted states. In Txnip-deficient mice, the levels appeared to be increased in both the fed and fasted states, although the results did not reach statistical significance, with P values of 0.22 and 0.23, respectively. In the fed state, the average leptin level in Txnip-deficient mice was 7.1 ng/ml, compared with the wild-type mice, which had 4.7 ng/ml. In the fasted state, the Txnip-deficient mice had an average leptin level of 3.4 ng/ml and the wild-type mice had an average level of 1.8 ng/ml. Increased plasma leptin would stimulate the esterification of fatty acids to be incorporated into triglycerides, which could explain the hypertriglyceridemia observed in Txnip-deficient mice.

Txnip influences glucose and fatty acid oxidation in the heart and skeletal muscle

As previously reported (2), Txnip is widely expressed, with high levels of mRNA in heart and muscle. Therefore, glucose and fatty acid oxidation were measured in isolated perfused heart, and fatty acid oxidation was measured in isolated soleus muscles. In the Txnip-deficient heart, glucose oxidation, as measured by the release of CO_2 from the oxidation of ^{14}C-labeled glucose, was substantially decreased (Fig. 1J). Rates of fatty acid oxidation were determined by measuring the amount of $^{3}H_2O$ released from

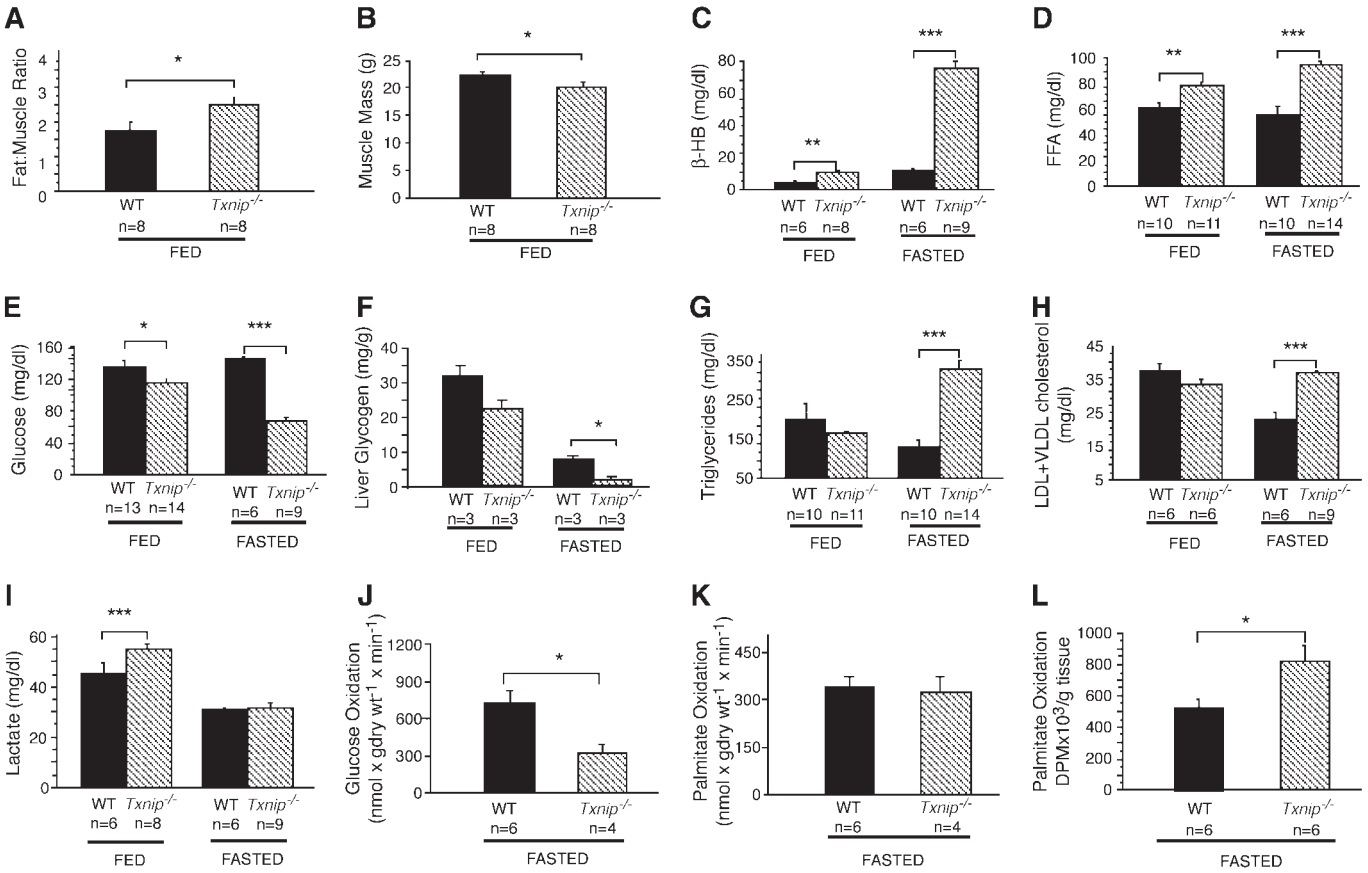

Fig. 1. In the fed state, thioredoxin-interacting protein (Txnip)-deficient mice exhibit an abnormal metabolic response to nutrition. C3H/DiSnA mice were used as the wild type (WT), indicated by solid bars, and Txnip-deficient (*Txnip*$^{-/-}$) mice, indicated by hatched bars, were fed a chow diet and water ad libitum. Blood and tissue samples were collected in the fed or fasted (18 h) state. For plasma lipid, glucose, and lactate levels, measurements are in mg/dl. A: Ratio of fat to lean muscle mass in the fed state by NMR spectroscopy. B: Muscle mass (g) in the fed state as determined by NMR spectroscopy. C: Ketone bodies measured as β-hydroxybutyrate (β-HB) levels. D: Plasma FFA levels. E: Plasma glucose levels. F: Liver glycogen. G: Plasma levels for triglycerides. H: LDL and VLDL cholesterol. I: Plasma lactate levels. J: Glucose oxidation was measured as the amount of ^{14}C-labeled CO_2 released upon incubation of hearts with [U-^{14}C]glucose. K: Palmitate oxidation was measured from $^{3}H_2O$ collected upon incubation of hearts with [9,10-^{3}H]palmitate. L: Palmitate oxidation of the soleus muscle using ^{14}C-labeled palmitate. * $P < 0.05$, ** $P < 0.01$, and *** $P < 0.001$. Data are presented as means ± SEM; number of mice (n) in each group is as indicated.

the oxidation of ^{3}H-labeled palmitate in the heart and the amount of $^{14}CO_2$ released from the oxidation of ^{14}C-labeled palmitate in the soleus muscle. There was no significant difference in fatty acid oxidation in the heart between the wild-type and Txnip-deficient mice (Fig. 1K). In wild-type hearts, fatty acid oxidation provided 64% of the acetyl-CoA for the TCA cycle, whereas in Txnip-deficient mouse hearts, 82% of the acetyl-CoA for the TCA cycle originated from fatty acids. The contribution of glucose oxidation and fatty acid oxidation to TCA cycle activity in the isolated working hearts was calculated using the following values: 2 mol of acetyl-CoA supplied to the TCA cycle from every 1 mol of glucose oxidized and 8 mol of acetyl-CoA supplied to the TCA cycle from every 1 mol of palmitate oxidized. This indicates that the Txnip-deficient heart is preferentially using fatty acids as a substrate over glucose.

We also measured fatty acid utilization in the soleus muscle in the fasted state by determining CO_2 release using ^{14}C-labeled palmitate as the substrate. Fatty acid oxidation was increased by 35% in the Txnip-deficient soleus muscle in the fasted state (Fig. 1L). According to the Randle hypothesis, increased plasma FFA could explain the increased fatty acid uptake in the muscle (18, 19).

Txnip deficiency alters the expression of PGC-1α and its downstream targets

To understand the molecular basis of the above metabolic perturbations resulting from the *Txnip* mutation, real-time quantitative PCR was used to analyze the expression of metabolic candidate genes in the liver, adipose, and skeletal muscle in the fed and fasted states. PGC-1α, a regulator of genes involved in gluconeogenesis, ketogenesis, and fatty acid oxidation, is induced in response to fasting (20). Txnip-deficient mice in the fed state showed a 5-fold increase in PGC-1α expression compared with wild-type mice in the fed state (**Fig. 2A**). When subjected to fasting, wild-type mice exhibited an increase in PGC-1α expression, whereas in Txnip-deficient mice, PGC-1α ex-

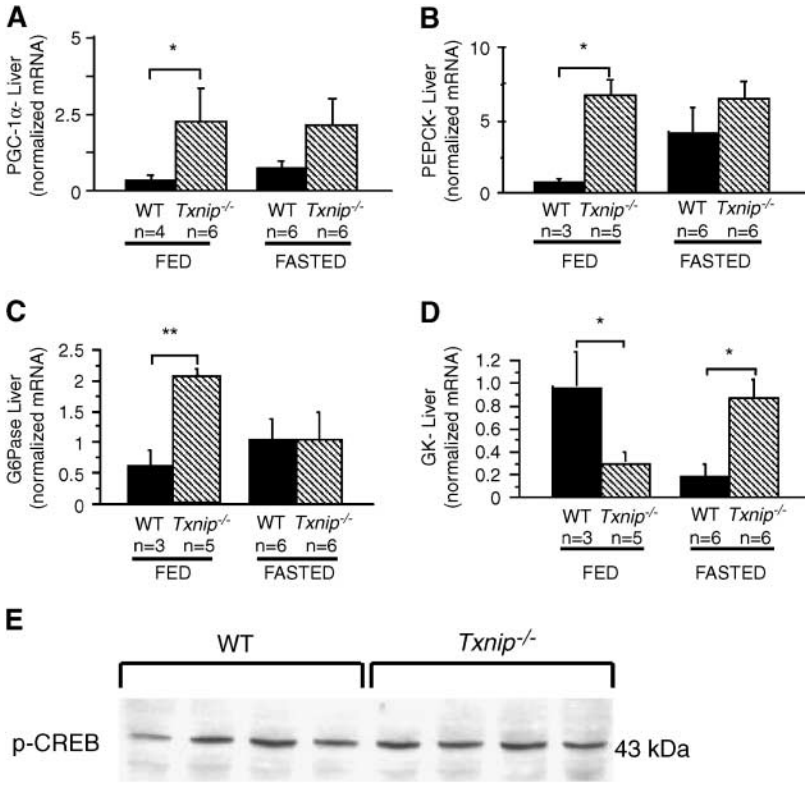

Fig. 2. Txnip deficiency induces expression changes of peroxisome proliferator-activated receptor-γ coactivator-1α (PGC-1α) and other key metabolic genes in the liver. Mice were either in the fed or fasted (18 h) state before liver RNA isolation. A: PGC-1α mRNA expression. B: Phosphoenolpyruvate carboxykinase (PEPCK) mRNA expression. C: Glucose-6-phosphatase (G6Pase) mRNA expression. D: Glucokinase (GK) mRNA expression. E: Liver protein levels of phosphorylated cAMP response element binding protein (p-CREB) in the fed state of wild-type and Txnip-deficient mice (n = 4 in each group) determined by Western blot analysis. RNA was analyzed by real-time quantitative PCR and normalized against 36B4 expression. Quantitative PCR results are averages of samples run in duplicate. C3H/DiSnA mice were used as the wild type (WT), indicated by solid bars, and Txnip-deficient (*Txnip*$^{-/-}$) mice are indicated by hatched bars. * $P < 0.05$ and ** $P < 0.01$. Data are presented as means ± SEM; number of mice (n) in each group is as indicated.

pression was unchanged but still slightly increased compared with wild-type mice (Fig. 2A).

Consistent with the known effects of PGC-1α on gluconeogenic genes (20), phosphoenolpyruvate carboxykinase (PEPCK) and glucose-6-phosphatase (G6Pase) were increased 10-fold and 3-fold, respectively, in the fed Txnip-deficient livers (Fig. 2B, C). Whereas PEPCK and G6Pase were induced in the fasted state of the wild-type mice, in the Txnip-deficient mice, the expression was unchanged or reduced relative to the fed state (Fig. 2B, C). The expression of glucokinase, which catalyzes the first step in glycolysis, was abnormal in Txnip-deficient mice; whereas wild-type mice exhibited a decrease in expression upon fasting Txnip-deficient mice showed an increase (Fig. 2D). Thus, the fact that Txnip-deficient mice exhibit a dysregulation in response to feeding can be explained in part by the altered expression of PGC-1α.

It has been shown that PGC-1α is regulated by insulin, glucocorticoids, and CREB (21). The entire family of Txn proteins activate CREB, with the highest activation occurring through the action of nucleoredoxin and glutaredoxin (22). Txnip binds to a conserved cysteine consensus sequence found in the Txn family, so it is feasible that Txnip could bind to other members. To determine whether the increase in PGC-1α in the fed state is the result of increased activation of CREB, we measured the protein levels of phosphorylated CREB (p-CREB) between Txnip-deficient and wild-type mice. We observed no significant difference in protein levels of p-CREB between Txnip-deficient and wild-type livers in the fed state (Fig. 2E). This suggests that the difference in PGC-1α expression may be occurring through an alternative mechanism.

Effects of Txnip deficiency on hepatic fatty acid metabolic enzymes

We previously showed that Txnip-deficient mice secrete more triglycerides from the liver, resulting in increased plasma levels of VLDL cholesterol, VLDL triglycerides, and both apolipoprotein B-100 and B-48 (1). To test whether this is attributable to increased fatty acid synthesis, we measured the expression of FAS in liver using real-time PCR. Although FAS expression was suppressed during fasting, in Txnip-deficient mice, FAS expression was increased compared with wild-type mice in both fed and fasting conditions (**Fig. 3A**). Because plasma triglycerides in Txnip-deficient mice are increased only during fasting (Fig.

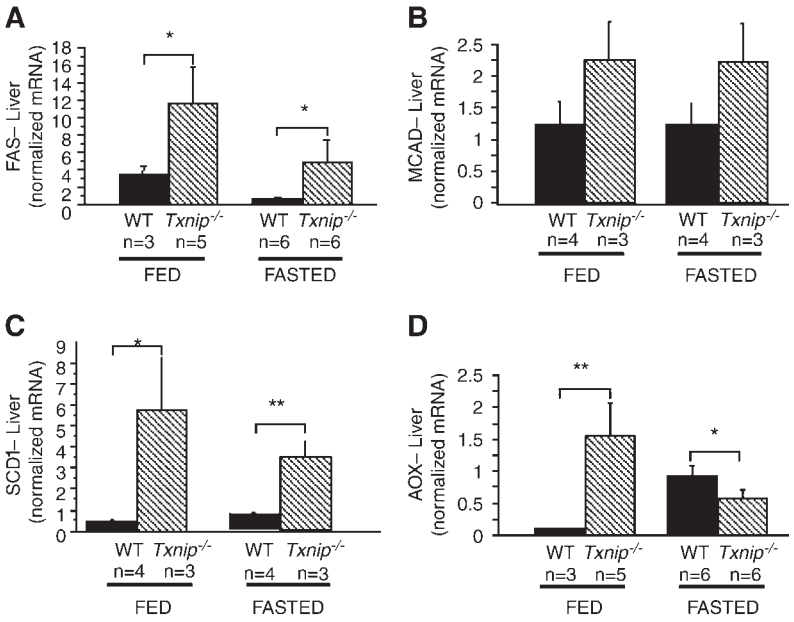

Fig. 3. Fatty acid metabolism genes show altered expression in the liver. Mice were either in the fed or fasted (18 h) state before liver RNA isolation. A: FAS mRNA expression. B: Medium-chain acyl-CoA dehydrogenase (MCAD) mRNA expression. C: Stearoyl-CoA desaturase 1 (SCD1) mRNA expression. D: Acyl-CoA oxidase (AOX) mRNA expression. RNA was analyzed by real-time quantitative PCR and normalized against 36B4 expression. Results are averages of samples run in duplicate. C3H/DiSnA mice were used as the wild type (WT), indicated by solid bars, and Txnip-deficient (*Txnip*$^{-/-}$) mice are indicated by hatched bars. * $P < 0.05$ and ** $P < 0.01$. Data are presented as means ± SEM; number of mice (n) in each group is as indicated.

1G), there are presumably other, compensatory changes during the fed state. To address this point, we measured the expression of enzymes involved in fatty acid metabolism. The Txnip-deficient mice appeared to have slightly increased expression of medium-chain acyl-CoA dehydrogenase (MCAD), which is involved in mitochondrial β-oxidation in both the fed and fasted states, although the levels did not reach statistical significance (Fig. 3B). Consistent with previous studies that show an increase in the activity of stearoyl-CoA desaturase 1 (SCD1) in fasted Txnip-deficient mice, we observed an increase in the fed and fasted levels of SCD1 mRNA (Fig. 3C) (23). It has been shown that SCD1 is a key regulator in determining the fate of fatty acids in the liver (24). Our results showing increased expression of SCD1 are consistent with this concept. We also measured acyl-CoA oxidase (AOX), an enzyme that catalyzes the first step of peroxisomal fatty acid oxidation and is an important target that is upregulated during fasting (25). In wild-type mice, AOX expression was increased during fasting (Fig. 3D). In Txnip-deficient mice, the enzyme level was already 10-fold increased in the fed state compared with wild-type mice (Fig. 3D). Thus, again, the profile of Txnip-deficient mice appears similar to that of the fasted animal.

Regulation of glucose metabolism by Txnip

The decrease in glucose levels during fasting (Fig. 1) suggests that there may be dysregulation of insulin production or responsiveness, and Hui et al. (8) observed significant differences in insulin levels between Txnip-deficient and wild-type mice in the fasted state. We measured insulin levels in several groups of mice in both the fed and fasted states using two different assay procedures, an ELISA (**Fig. 4A**) and a radioimmunoassay (data not shown). Although there was a trend toward increased levels of insulin in both the fed and fasted states, the differences were not statistically significant (Fig. 4A). The more modest increase in insulin levels may be attributable to the differ-

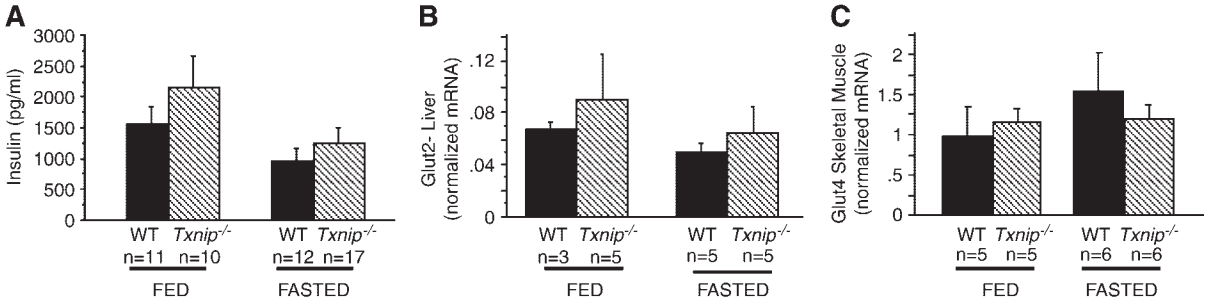

Fig. 4. Expression of insulin-responsive genes was not affected by Txnip deficiency. Plasma insulin and expression levels in skeletal muscle and liver in the fed and fasted states. A: Plasma insulin levels (pg/ml). B: Glucose transporter 2 (Glut2) mRNA expression in the liver. C: Glut4 mRNA expression in skeletal muscle. Insulin levels were measured by ELISA. RNA was analyzed by real-time quantitative PCR and normalized against 36B4 expression. Results are averages of samples run in duplicate. C3H/DiSnA mice were used as the wild type (WT), indicated by solid bars, and Txnip-deficient (*Txnip*$^{-/-}$) mice are indicated by shaded bars. Data are presented as means ± SEM; number of mice (n) in each group is as indicated.

ence in the age of the mice used in the previous study (6 months) compared with the mice used in this study (3–5 months) (8). To examine whether alterations in glucose metabolism resulted from altered expression of glucose transporters, we measured the expression of glucose transporter 2 (Glut2) in liver and Glut4 in muscle. No significant differences in either transporter were observed in the fed and fasted states (Fig. 4B, C). The expression of Glut4 was also unchanged in white adipose tissue (see below).

Tissue-specific dysregulation of genes in adipose tissue and skeletal muscle of Txnip-deficient mice

PGC-1α is important in adipose tissue metabolism. For example, it is induced in response to cold and regulates adaptive thermogenesis in brown adipose tissue (26). We examined PGC-1α mRNA expression in white adipose tissue from the gonadal fat pads. In the fed state, Txnip-deficient mice had decreased levels of PGC-1α mRNA compared with wild-type mice, and unlike in wild-type mice, PGC-1α mRNA levels did not decrease upon fasting (**Fig. 5A**).

The effect of Txnip deficiency on adipose metabolism was further examined by measuring mRNA levels of FAS and Glut4. In the fed state, the levels of FAS in adipose were substantially decreased in Txnip-deficient mice. The gene expression patterns of PGC-1α and FAS in the Txnip-deficient adipose tissue were significantly different from those seen in the liver. Although PGC-1α mRNA levels in the Txnip-deficient adipose tissue increased in the fasted state, the levels remained constitutively high between the fed and fasted states in the Txnip-deficient liver. FAS mRNA expression patterns were also significantly different between the Txnip-deficient adipose tissue and liver. Regardless of whether the Txnip-deficient mice were fed or fasted, the FAS levels in the adipose tissue were extremely low. However, in the Txnip-deficient liver, the FAS levels increased upon fasting. This indicates that the Txnip deficiency has opposing effects on the adipose tissue and the liver. In contrast to PGC-1α and FAS expression, mRNA levels of Glut4 in adipose tissue were unchanged between wild-type and Txnip-deficient mice (Fig. 5B, C).

One characteristic response of adipose tissue to fasting is an increased expression of tumor necrosis factor-α (TNFα), which is involved in the stimulation of lipolysis (27). In Txnip-deficient mice, TNFα levels were higher in the fed state (10-fold) and significantly lower than the wild-type levels in the fasted state (Fig. 5D). Thus, in adipose tissue as well as liver, fed Txnip-deficient mice exhibited an abnormal response to nutritional signals.

We also examined the expression of PGC-1α and AOX in the white skeletal muscle. PGC-1α expression in white muscles of the leg was not significantly affected by Txnip deficiency under fed or fasted conditions (Fig. 5E). AOX levels in Txnip-deficient mice were decreased in the fed state and were not significantly different in the fasted state (Fig. 5F). Because AOX is primarily involved in peroxisomal fatty acid oxidation, the unchanged level of AOX in the fasted Txnip-deficient mice is not inconsistent with the observed increase in palmitate oxidation in the soleus muscle.

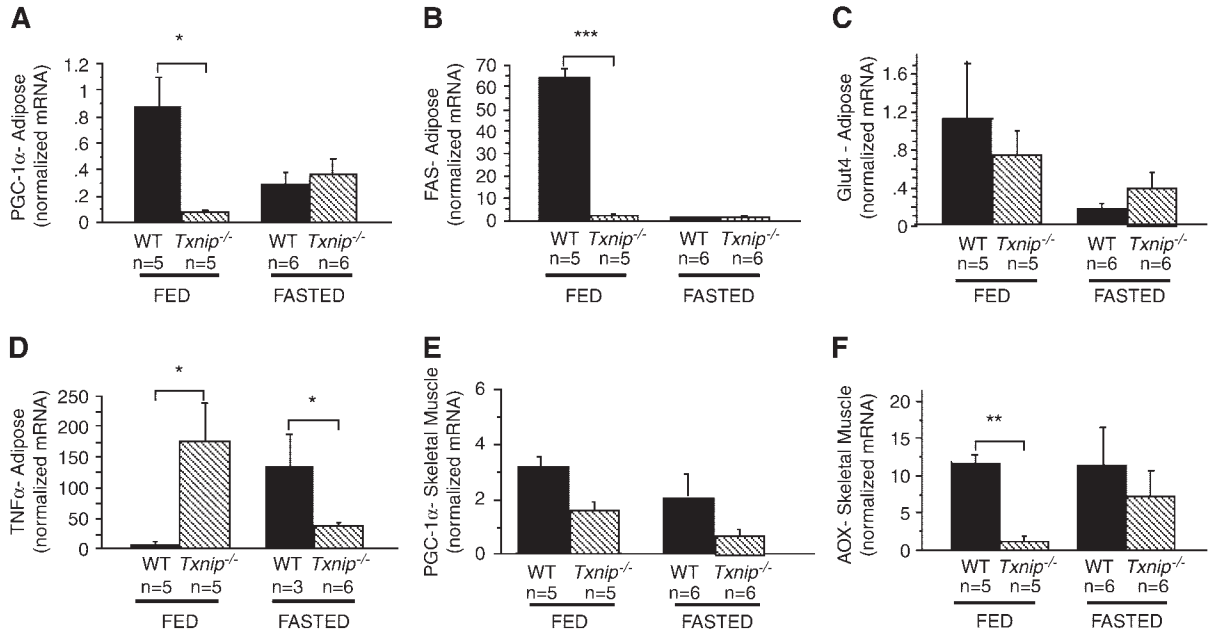

Fig. 5. PGC-1α and genes involved in lipid metabolism show altered expression in adipose and skeletal muscle. Mice were either fed or fasted for 18 h before RNA isolation of gonadal fat pads and skeletal muscle. A: PGC-1α mRNA expression in adipose tissue. B: FAS mRNA expression in adipose tissue. C: Glut4 mRNA expression in adipose tissue. D: Tumor necrosis factor-α (TNFα) mRNA expression in adipose tissue. E: PGC-1α mRNA expression in skeletal muscle. F: AOX mRNA expression in skeletal muscle. RNA was analyzed by real-time quantitative PCR and normalized against 36B4 expression. Results are averages of samples run in duplicate. C3H/DiSnA mice were used as the wild type (WT), indicated by solid bars, and Txnip-deficient (*Txnip*$^{-/-}$) mice are indicated by hatched bars. * $P < 0.05$, ** $P < 0.01$, and *** $P < 0.001$. Data are presented as means ± SEM; number of mice (n) in each group is as indicated.

Redox status of Txnip-deficient mice

We previously proposed that Txnip deficiency would result in increased levels of reduced pyridine nucleotides and that this would result in inhibition of flux through the TCA cycle, thereby sparing fatty acids for incorporation into triglycerides (2). To test this hypothesis, we quantitated the levels of these reduced and oxidized pyridine nucleotides using an HPLC assay (16). **Figure 6** shows the chromatograms and ratios between the pyridine nucleotides in the Txnip-deficient and wild-type mice. In the fed state, Txnip-deficient mice had a 2-fold increase in the ratio of NADH to NAD^+, although there were no statistically significant differences observed between Txnip-deficient and wild-type mice in the fasted state (Fig. 6C). The peaks for $NADP^+$ were too small given our background to reliably estimate the NADPH/$NADP^+$ ratio (Fig. 6). The determined levels (μmol/g) of NADH and NAD^+, respectively, were: 0.034 ± 0.001 and 0.219 ± 0.021 (wild type, fed); 0.045 ± 0.003 and 0.134 ± 0.007 (Txnip deficient, fed); 0.038 ± 0.004 and 0.180 ± 0.005 (wild type, fasted); 0.024 ± 0.002 and 0.123 ± 0.011 (Txnip deficient, fasted). Although these data are consistent with our observation that Txnip-deficient mice show a metabolic dysregulation in the fed state, the change in NADH/NAD^+ ratio does not appear to be able to explain the metabolic perturbations of Txnip deficiency in the fasted state.

Txn may not mediate the effects of the Txnip deficiency

In vitro studies suggest that Txnip acts as a negative regulator of Txn activity and protein levels (15). In cells transfected with *Txnip*, Txn activity was reduced by 50%. However, after upregulating *Txnip* 9-fold upon 1,25-dihydroxyvitamin D_3 treatment in HL-60 cells, there was only a modest decrease in Txn activity (15). Because the critical binding region of Txnip was absent in our mutant mice and Txnip mRNA was greatly reduced, we expected that our mice would exhibit enhanced expression and activity of Txn in vivo. We measured the hepatic protein levels of Txn in the fed and fasted states. The activity of Txn was also measured in the fed and fasted liver by detecting the amount of reduced insulin in an enzymatic assay, as previously described (17). Surprisingly, the protein level (**Fig. 7A**) and activity of Txn (Fig. 7B) were not discernibly different between Txnip-deficient mice and wild-type mice in either the fed or fasted states. These data suggest that the metabolic perturbations in Txnip-deficient mice may involve other interactions as well.

DISCUSSION

We previously used positional cloning to identify *Txnip* as the gene underlying hypertriglyceridemia in a naturally

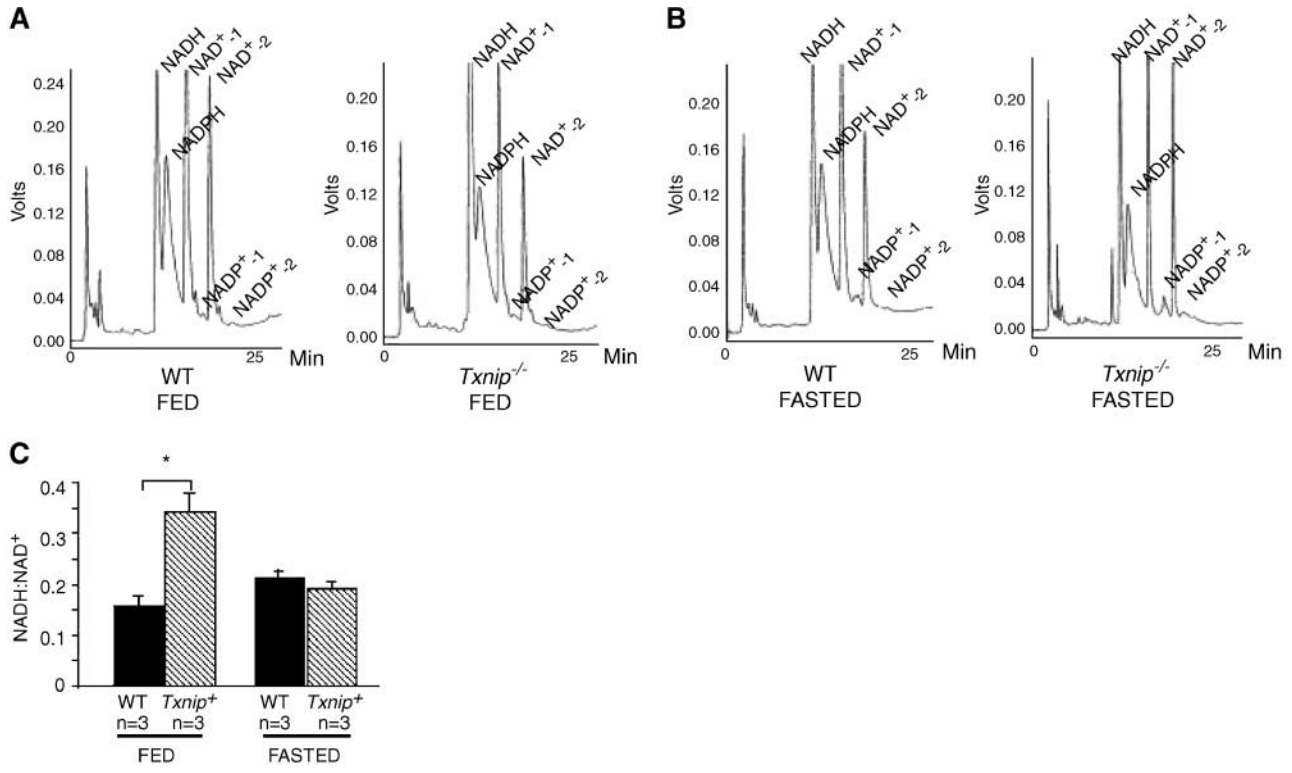

Fig. 6. Redox state is altered in Txnip-deficient mice in the fed state. A: Representative HPLC elution profiles image of pyridine dinucleotides in fed liver tissue (75 mg). B: Representative HPLC elution profiles of pyridine dinucleotides in fasted liver tissue (75 mg). C: NADH/NAD^+ molar ratio in fed and fasted mice. Reaction of oxidized pyridine nucleotides with cyanide leads to two stable fluorescent products (NAD^+-1, NAD^+-2, $NADP^+$-1, $NADP^+$-2) resulting in the separation of four nucleotides in one chromatogram and the generation of six peaks in the following order: NADH, NADPH, NAD^+-1, $NADP^+$-1, NAD^+-2, $NADP^+$-2. C3H/HeJ mice were used as the wild type (WT), indicated by solid bars, and Txnip-deficient (*Txnip*$^{-/-}$) mice are indicated by shaded bars. * $P < 0.05$. Data are presented as means ± SEM; number of mice (n) in each group is as indicated.

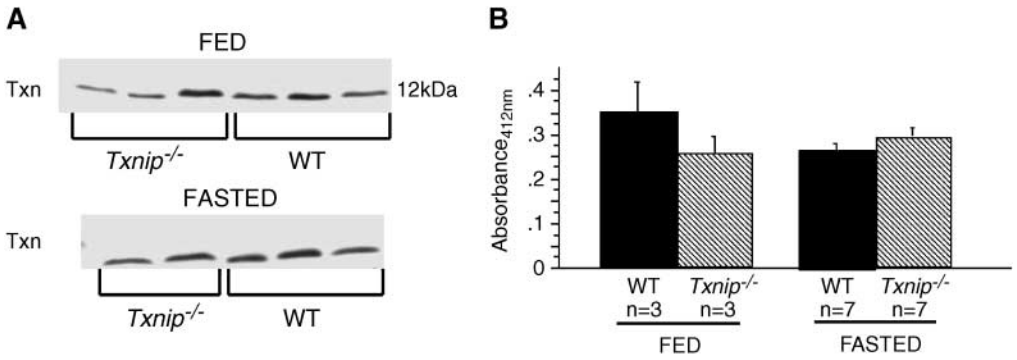

Fig. 7. Txnip deficiency may not mediate effects through thioredoxin (Txn). Western blot analysis of Txn and insulin-reducing activity in liver. A: Liver protein levels of Txn in Txnip-deficient and wild-type mice in the fed and fasted states. B: Txn activity in liver measured by insulin-reducing assay in Txnip-deficient and wild-type mice in the fed and fasted states. Reduced insulin was measured at an absorbance of 412 nm. Results are averages of samples run in duplicate. Data shown are representative of two independent experiments. C3H/DiSnA mice were used as the wild type (WT), indicated by solid bars, and Txnip-deficient (*Txnip*$^{-/-}$) mice are indicated by hatched bars. Data are presented as means ± SEM; number of mice (n) in each group is as indicated.

occurring mouse model (2). We have now examined in detail the metabolic perturbations resulting from Txnip deficiency. Several conclusions have emerged from these studies. First, Txnip deficiency results in a disruption in the fasting-feeding metabolic transition, perturbing glucose as well as lipid metabolism in a variety of tissues. Second, the deficiency is associated with large alterations in the expression of key metabolic enzymes and regulators, including altered expression of PGC-1α in liver and adipose. Third, there is an altered redox status in the livers of Txnip-deficient mice, which may be the cause or the result of the metabolic abnormalities observed in Txnip-deficient mice. Furthermore, the fact that Txn activity was not significantly affected raises the possibility of other interactions.

The normal response to prolonged fasting is increased lipolysis of adipose triglycerides, release of fatty acids into the circulation, and uptake of fatty acids by liver and other tissues, where they can be oxidized. During fasting, the liver exhibits increased gluconeogenesis and increased production of ketone bodies, which can be used by the brain, skeletal muscle, cardiac muscle, and other tissues as a source of energy. Plasma levels of glucose and triglycerides normally decrease in a fasted state. In the fed state, Txnip-deficient mice exhibit many of the characteristics of the fasted state, including increased ketone bodies, decreased glucose levels, and increased plasma FFA (Fig. 1). The lower hepatic glycogen levels seen in the fasted Txnip-deficient mice can be explained in part by a trend ($P = 0.07$) toward lower glycogen in the fed state. Because the Txnip-deficient mice already have a depleted source of glycogen in the fed state, the fasted levels are much lower. Ntambi et al. (24) have shown that SCD1 deficiency leads to increased fatty acid oxidation and decreased triglyceride synthesis along with decreased leptin levels. The increased expression and activity of SCD1 in fasted Txnip-deficient mice suggests that Txnip deficiency may control the fate of fatty acids in the liver through SCD1 (23). The lack of a significant difference in MCAD mRNA expression levels also suggests that the dysregulation leading to increased ketone body production and decreased CO_2 production in the Txnip-deficient livers occurs downstream of β-oxidation. The adipose tissue of fed Txnip-deficient mice also exhibited characteristics of a fasted state; in particular, the Txnip-deficient mice had dramatically (10-fold) increased expression of TNFα in the fed state (Fig. 5D). In the Txnip-deficient adipose tissue, the expression levels of metabolic genes, such as PGC-1α and FAS, were significantly different from levels observed in the Txnip-deficient liver, indicating tissue-specific effects.

One of the fundamental regulatory molecules involved in the response to fasting is PGC-1α. This transcriptional coactivator is involved in nutritional and other environmental responses in liver, muscle, and adipose tissue (20, 28, 29). Whereas PGC-1α is normally induced in liver in response to fasting, Txnip-deficient mice in the fed state had PGC-1α levels exceeding those of fasted wild-type mice (Fig. 2A). Furthermore, the known downstream targets of PGC-1α, such as PEPCK and G6Pase, also exhibited similar changes in expression levels (Fig. 2B, C).

Several recent studies have identified Txnip as a potential key regulator of glucose homeostasis. Thus, *Txnip* expression is dramatically upregulated in isolated pancreatic β cells upon exposure to glucose (30). In rat fibroblasts treated with glucose, *Txnip* induction occurs even in the presence of cycloheximide, implying that *Txnip* is a glucose-responsive immediate early gene (31). Recent studies showed that streptozotocin treatment of Txnip-deficient mice reduced the hypertriglyceridemia phenotype in the fasted state, implying that the effects of Txnip are mediated in part by insulin levels (8). Hui et al. (8) supported this conclusion by showing that, in the fasted state, insulin levels were increased in Txnip-deficient mice and that the level of the insulin-inducible transcription factor SREBP-1c was increased in fasted Txnip-deficient mice. In our present study, we observed a trend toward increased insulin levels in both fed and fasted states (Fig. 4A), but these were not statistically significant. This could be explained, in part, by the difference in the ages of the animals used in this study and the larger sample size. To test

for possible methodological problems, we used two different assays, radioimmunoassay (data not shown) and ELISA. Recently, Schulze et al. (9) presented evidence that the oxidative stress contributing to the complications of diabetes may result in part from the induction of Txnip by increased glucose.

Our studies and two other recent studies agree in finding that the hyperlipidemic phenotype of Txnip-deficient mice is attributable, at least in part, to increased triglyceride synthesis resulting from increased expression of fatty acid synthase. This is probably mediated in large part by increased expression of the key lipogenic transcription factor SREBP-1c (8). The mechanism leading to the reduced glucose levels in fasted Txnip-deficient mice will require additional biochemical and kinetic studies. Our studies do not provide evidence of decreased hepatic glucose synthesis or increased glucose utilization by peripheral tissues. One possible explanation, supported by increased plasma lactate levels in the fed state, is increased Cori cycling.

The cellular redox state is critical for maintaining homeostasis, and we have now demonstrated that Txnip influences the levels of NADH. This is likely to have a broad metabolic impact. For example, reduced pyridine nucleotides promote, whereas oxidized pyridine nucleotides inhibit, the binding of transcription factors for genes involved in the circadian clock (32). Also, there is evidence that an increased NADH/NAD^+ ratio promotes the conversion of pyruvate to lactate (33) and that $NADP^+$ inhibits gluconeogenesis (34). Consistent with this, our results show an increase in plasma lactate and hepatic gluconeogenic enzymes in the fed state of Txnip-deficient mice. However, since there were no significant changes in the ratios of reduced-to-oxidized pyridine in the fasted state, the altered redox state does not explain the changes seen in fasted Txnip-deficient mice. It is noteworthy that hepatic ratios of reduced-to-oxidized glutathione were increased by 30% in Txnip-deficient mice in the fasted state (8).

Our data suggest the Txnip deficiency alters the metabolism in various tissues. However, our results suggest that the effects are not mediated entirely by Txn, because we failed to observe significant changes in Txn levels or in Txn activity in Txnip-deficient mice. We hypothesize that Txnip may interact with other members of the Txn family, including glutaredoxin and nucleoredoxin, all of which have the CXXC motif by which Txnip is thought to interact with Txn (22, 35). Recently, Yodoi and colleagues (36) used a yeast two-hybrid screen to identify additional proteins that interact with Txnip. Among these is importin α1, which facilitates the transport of Txnip into the nucleus (36). It is clear that the nonsense mutation of *Txnip* we have studied here would not interact with Txn. In studies with truncated Txnip, it has been shown that amino acids 134–395 of Txnip were required for Txn binding and inhibition of activity (35). Because the nonsense mutation of *Txnip* occurs at amino acid 97 (2), the critical binding region of Txnip is absent. Moreover, because of nonsense-mediated RNA decay, the mRNA levels of the mutant *Txnip* transcript were greatly decreased (2).

In conclusion, our results indicate that the normal changes in glucose and fatty acid metabolism in response to feeding are dependent upon *Txnip* expression. The mechanism appears to be mediated in part by effects on the redox status of cells, but precisely how redox status affects key transcription factors and enzymes involved in the metabolism of lipids and glucose is unclear. It is also possible that the altered redox status is a consequence rather than a cause of some of these metabolic perturbations.

This study was supported by National Institutes of Health Grants HL-28481 (A.J.L.) and HL-30568 (P.T.) and by the Canadian Institutes of Health Research (G.D.L.). S.C. was supported in part by National Institutes of Health Training Grant T32-HL-069766.

REFERENCES

1. Castellani, L. W., A. Weinreb, J. Bodnar, A. M. Goto, M. Doolittle, M. Mehrabian, P. Demant, and A. J. Lusis. 1998. Mapping a gene for combined hyperlipidaemia in a mutant mouse strain. *Nat. Genet.* **18:** 374–377.
2. Bodnar, J. S., A. Chatterjee, L. W. Castellani, D. A. Ross, J. Ohmen, J. Cavalcoli, C. Wu, K. M. Dains, J. Catanese, M. Chu, S. S. Sheth, K. Charugundla, P. Demant, D. B. West, P. de Jong, and A. J. Lusis. 2002. Positional cloning of the combined hyperlipidemia gene Hyplip1. *Nat. Genet.* **30:** 110–116.
3. Gasdaska, J. R., M. Berggren, and G. Powis. 1995. Cell growth stimulation by the redox protein thioredoxin occurs by a novel helper mechanism. *Cell Growth Differ.* **6:** 1643–1650.
4. Hirota, K., M. Matsui, S. Iwata, A. Nishiyama, K. Mori, and J. Yodoi. 1997. AP-1 transcriptional activity is regulated by a direct association between thioredoxin and Ref-1. *Proc. Natl. Acad. Sci. USA.* **94:** 3633–3638.
5. Nakamura, H., K. Nakamura, and J. Yodoi. 1997. Redox regulation of cellular activation. *Annu. Rev. Immunol.* **15:** 351–369.
6. Ueda, S., H. Nakamura, H. Masutani, T. Sasada, S. Yonehara, A. Takabayashi, Y. Yamaoka, and J. Yodoi. 1998. Redox regulation of caspase-3(-like) protease activity: regulatory roles of thioredoxin and cytochrome c. *J. Immunol.* **161:** 6689–6695.
7. Donnelly, K. L., M. R. Margosian, S. S. Sheth, A. J. Lusis, and E. J. Parks. 2004. Increased lipogenesis and fatty acid reesterification contribute to hepatic triacylglycerol stores in hyperlipidemic Txnip−/− mice. *J. Nutr.* **134:** 1475–1480.
8. Hui, T. Y., S. S. Sheth, J. M. Diffley, D. W. Potter, A. J. Lusis, A. D. Attie, and R. A. Davis. 2004. Mice lacking thioredoxin-interacting protein provide evidence linking cellular redox state to appropriate response to nutritional signals. *J. Biol. Chem.* **279:** 24387–24393.
9. Schulze, P. C., J. Yoshioka, T. Takahashi, Z. He, G. L. King, and R. T. Lee. 2004. Hyperglycemia promotes oxidative stress through inhibition of thioredoxin function by thioredoxin-interacting protein. *J. Biol. Chem.* **279:** 30369–30374.
10. Demant, P., and A. A. Hart. 1986. Recombinant congenic strains—a new tool for analyzing genetic traits determined by more than one gene. *Immunogenetics.* **24:** 416–422.
11. Hedrick, C. C., L. W. Castellani, C. H. Warden, D. L. Puppione, and A. J. Lusis. 1993. Influence of mouse apolipoprotein A-II on plasma lipoproteins in transgenic mice. *J. Biol. Chem.* **268:** 20676–20682.
12. Campbell, F. M., R. Kozak, A. Wagner, J. Y. Altarejos, J. R. Dyck, D. D. Belke, D. L. Severson, D. P. Kelly, and G. D. Lopaschuk. 2002. A role for peroxisome proliferator-activated receptor alpha (PPAR-alpha) in the control of cardiac malonyl-CoA levels: reduced fatty acid oxidation rates and increased glucose oxidation rates in the hearts of mice lacking PPARalpha are associated with higher concentrations of malonyl-CoA and reduced expression of malonyl-CoA decarboxylase. *J. Biol. Chem.* **277:** 4098–4103.
13. Olubadewo, J., D. W. Morgan, and M. Heimberg. 1983. Effects of triiodothyronine on biosynthesis and secretion of triglyceride by

livers perfused in vitro with [^{3}H]oleate and [^{14}C]glycerol. *J. Biol. Chem.* **258:** 938–945.
14. Laffitte, B. A., S. B. Joseph, R. Walczak, L. Pei, D. C. Wilpitz, J. L. Collins, and P. Tontonoz. 2001. Autoregulation of the human liver X receptor alpha promoter. *Mol. Cell. Biol.* **21:** 7558–7568.
15. Nishiyama, A., M. Matsui, S. Iwata, K. Hirota, H. Masutani, H. Nakamura, Y. Takagi, H. Sono, Y. Gon, and J. Yodoi. 1999. Identification of thioredoxin-binding protein-2/vitamin D(3) up-regulated protein 1 as a negative regulator of thioredoxin function and expression. *J. Biol. Chem.* **274:** 21645–21650.
16. Adams, J. D., Jr., and L. K. Klaidman. 2002. Oxidative stress and nicotinamide effects on brain pyrimidine nucleotides. *Recent Research and Development in Analytical Biochemistry.* **2:** 249–264.
17. Holmgren, A., and M. Bjornstedt. 1995. Thioredoxin and thioredoxin reductase. *Methods Enzymol.* **252:** 199–208.
18. Randle, P. J., P. B. Garland, C. N. Hales, and E. A. Newsholme. 1963. The glucose fatty-acid cycle. Its role in insulin sensitivity and the metabolic disturbances of diabetes mellitus. *Lancet.* **1:** 785–789.
19. Jequier, E. 1998. Effect of lipid oxidation on glucose utilization in humans. *Am. J. Clin. Nutr.* **67 (Suppl. 3):** 527–530.
20. Yoon, J. C., P. Puigserver, G. Chen, J. Donovan, Z. Wu, J. Rhee, G. Adelmant, J. Stafford, C. R. Kahn, D. K. Granner, C. B. Newgard, and B. M. Spiegelman. 2001. Control of hepatic gluconeogenesis through the transcriptional coactivator PGC-1. *Nature.* **413:** 131–138.
21. Herzig, S., F. Long, U. S. Jhala, S. Hedrick, R. Quinn, A. Bauer, D. Rudolph, G. Schutz, C. Yoon, P. Puigserver, B. Spiegelman, and M. Montminy. 2001. CREB regulates hepatic gluconeogenesis through the coactivator PGC-1. *Nature.* **413:** 179–183.
22. Hirota, K., M. Matsui, M. Murata, Y. Takashima, F. S. Cheng, T. Itoh, K. Fukuda, and J. Yodoi. 2000. Nucleoredoxin, glutaredoxin, and thioredoxin differentially regulate NF-kappaB, AP-1, and CREB activation in HEK293 cells. *Biochem. Biophys. Res. Commun.* **274:** 177–182.
23. Attie, A. D., R. M. Krauss, M. P. Gray-Keller, A. Brownlie, M. Miyazaki, J. J. Kastelein, A. J. Lusis, A. F. Stalenhoef, J. P. Stoehr, M. R. Hayden, and J. M. Ntambi. 2002. Relationship between stearoyl-CoA desaturase activity and plasma triglycerides in human and mouse hypertriglyceridemia. *J. Lipid Res.* **43:** 1899–1907.
24. Ntambi, J. M., M. Miyazaki, J. P. Stoehr, H. Lan, C. M. Kendziorski, B. S. Yandell, Y. Song, P. Cohen, J. M. Friedman, and A. D. Attie. 2002. Loss of stearoyl-CoA desaturase-1 function protects mice against adiposity. *Proc. Natl. Acad. Sci. USA.* **99:** 11482–11486.
25. Hashimoto, T., W. S. Cook, C. Qi, A. V. Yeldandi, J. K. Reddy, and M. S. Rao. 2000. Defect in peroxisome proliferator-activated receptor alpha-inducible fatty acid oxidation determines the severity of hepatic steatosis in response to fasting. *J. Biol. Chem.* **275:** 28918–28928.
26. Puigserver, P., Z. Wu, C. W. Park, R. Graves, M. Wright, and B. M. Spiegelman. 1998. A cold-inducible coactivator of nuclear receptors linked to adaptive thermogenesis. *Cell.* **92:** 829–839.
27. Green, A., J. M. Rumberger, C. A. Stuart, and M. S. Ruhoff. 2004. Stimulation of lipolysis by tumor necrosis factor-alpha in 3T3-L1 adipocytes is glucose dependent: implications for long-term regulation of lipolysis. *Diabetes.* **53:** 74–81.
28. Rhee, J., Y. Inoue, J. C. Yoon, P. Puigserver, M. Fan, F. J. Gonzalez, and B. M. Spiegelman. 2003. Regulation of hepatic fasting response by PPARgamma coactivator-1alpha (PGC-1): requirement for hepatocyte nuclear factor 4alpha in gluconeogenesis. *Proc. Natl. Acad. Sci. USA.* **100:** 4012–4017.
29. Puigserver, P., and B. M. Spiegelman. 2003. Peroxisome proliferator-activated receptor-gamma coactivator 1 alpha (PGC-1 alpha): transcriptional coactivator and metabolic regulator. *Endocr. Rev.* **24:** 78–90.
30. Shalev, A., C. A. Pise-Masison, M. Radonovich, S. C. Hoffmann, B. Hirshberg, J. N. Brady, and D. M. Harlan. 2002. Oligonucleotide microarray analysis of intact human pancreatic islets: identification of glucose-responsive genes and a highly regulated TGFbeta signaling pathway. *Endocrinology.* **143:** 3695–3698.
31. Hirota, T., T. Okano, K. Kokame, H. Shirotani-Ikejima, T. Miyata, and Y. Fukada. 2002. Glucose down-regulates Per1 and Per2 mRNA levels and induces circadian gene expression in cultured Rat-1 fibroblasts. *J. Biol. Chem.* **277:** 44244–44251.
32. Rutter, J., M. Reick, L. C. Wu, and S. L. McKnight. 2001. Regulation of clock and NPAS2 DNA binding by the redox state of NAD cofactors. *Science.* **293:** 510–514.
33. Ferraz, M., K. Brunaldi, C. E. Oliveira, and R. B. Bazotte. 1997. Hepatic glucose production from L-alanine is absent in perfused liver of diabetic rats. *Res. Commun. Mol. Pathol. Pharmacol.* **95:** 147–155.
34. Fulgencio, J. P., C. Kohl, J. Girard, and J. P. Pegorier. 1996. Troglitazone inhibits fatty acid oxidation and esterification, and gluconeogenesis in isolated hepatocytes from starved rats. *Diabetes.* **45:** 1556–1562.
35. Junn, E., S. H. Han, J. Y. Im, Y. Yang, E. W. Cho, H. D. Um, D. K. Kim, K. W. Lee, P. L. Han, S. G. Rhee, and I. Choi. 2000. Vitamin D3 up-regulated protein 1 mediates oxidative stress via suppressing the thioredoxin function. *J. Immunol.* **164:** 6287–6295.
36. Nishinaka, Y., H. Masutani, S. I. Oka, Y. Matsuo, Y. Yamaguchi, K. Nishio, Y. Ishii, and J. Yodoi. 2004. Importin alpha 1 (Rch1) mediates nuclear translocation of thioredoxin-binding protein-2 (TBP-2/VDUP1). *J. Biol. Chem.* **279:** 37559–37565.